Biomechanical properties of soft tissue measurement using Optical Coherence Elastography

Marjan Razani[1], Adrian Mariampillai[2], Cuiru Sun[2], Victor X.D. Yang[2,3], Michael C. Kolios[1]
(1) Department of Physics, Ryerson University, Toronto, Canada
(2) Department of Electrical and Computer Engineering, Ryerson University, Toronto, Canada
(3) Division of Neurosurgery, University of Toronto, Toronto, Canada

Abstract

Optical Coherence Tomography (OCT) provides images at near histological resolution, which allows for the identification of micron sized morphological tissue structures. Optical coherence elastography (OCE) measures tissue displacement and utilizes the high resolution of OCT to generate high-resolution stiffness maps. In this work, we explored the potential of measuring shear wave propagation using OCE. A swept-source OCT system was used in this study. The laser had a center wavelength of 1310 nm and a bandwidth of ~110 nm. The lateral resolution was approximately 13 μm in the samples. Acoustic radiation force was applied to two different phantoms using a 20 MHz circular 8.5 mm diameter piezoelectric transducer element (PZT, f-number 2.35) transmitting sine-wave bursts of 400 μs. The first phantom consisted of a 355 μm glass sphere (dark) embedded in gelatin that was used to characterize the ultrasound pushing beam. The second consisted of gelatin mixed with titanium dioxide, which provided uniform acoustic and optical scattering. The OCT signal from this second set of phantoms was used for the measurement of the shear wave speed and viscosity. For both sets of experiments phase analysis was applied to B-mode and M-mode OCT images which were obtained while the ultrasound transducer was generating the "push" in the phantom. The experiments are the first step towards imaging shear wave propagation in tissue and characterization of tissue mechanical properties using OCE, with the eventual goal of developing OCE as a diagnostic tool for the assessment of pathological lesions with different mechanical tissue property.

Keywords: Shear wave, Elastography, Optical coherence Tomography, Acoustic Radiation Force, mechanical properties.

1. Introduction

Elastography is a method in which stiffness or strain images of soft tissue are generated for diagnostic purposes [1]. An imaging modality is used to image tissue deformation behavior under a static or dynamic load and ultimately generate images called elastograms. Elastograms contain information about local variations of the stiffness inside a region of interest and may provide additional clinical information to aid in the identification of suspicious lesions, the diagnosis of various disease states and the monitoring of the effectiveness of treatments. Different imaging modalities can be used to measure tissue displacements and estimate the resulting tissue mechanical properties such as ultrasound or magnetic resonance (MR) imaging [2]. The drawbacks of MRI are that it is technologically complex, expensive and has long clinical wait times. Moreover, both MRI and ultrasound do not have sufficient resolution to detect small and subtle elastic variations in tissue such as in small tumors and atherosclerotic plaques. Optical Coherence Tomography (OCT) is an optical tomographic imaging technique that shares many similarities to ultrasound imaging despite using light. OCT has several advantages over other imaging modalities, primarily due to its inherently high resolution, which allows for the identification of micron sized morphological tissue structures. This increased resolution comes at the expense of limited imaging penetration depth, which is on the order of a few millimeters. The technology is also flexible and inexpensive. Optical coherence elastography (OCE) measures tissue displacement using OCT and benefits from the high resolution of this imaging technology. OCE is a relatively new elastography technology used to measure biomechanical properties of soft tissue [3]. During OCE, the tissue can be excited internally or externally and statically or dynamically [4]. Methods of creating dynamic compressions include acoustic radiation force (ARF) and low-frequency vibration [5].

Photonic Therapeutics and Diagnostics VIII, edited by Nikiforos Kollias, et al., Proc. of SPIE Vol. 8207, 820758 · © 2012 SPIE · CCC code: 0277-786X/12/$18 · doi: 10.1117/12.920736

To assess mechanical properties of tissues, there are several research groups that are investigating the use of acoustic radiation force excitation to produce the transient excitations. Acoustic radiation force imaging is used in general elasticity imaging methods [6-10], for the characterization of lesions [11, 22], muscle screening [12], and imaging the calcification of arteries [13]. Most of the researchers are investigating methods to measure the mechanical properties of tissue using external excitation of the tissue [14]. To calculate the mechanical properties the tissue shear wave speed was measured. This approach assumes that the shear wave propagates in homogeneous tissue. There are several ways that the speed of the shear wave can be measured. These methods include the inversion of the Helmholtz equation which characterizes the shear wave propagation [15, 16], lateral time to-peak displacement algorithms [21], tracking displacement field jitter that is associated with shear waves [17, 18] and a variety of correlation-based algorithms [19, 20]. The speed of the shear waves that propagate in the soft tissue is directly related to the shear modulus of the material [21, 22]. Traditional compression wave imaging, such as ultrasound elastography, provides measurements based on the tissue bulk modulus, which is confined to a relatively small range for soft tissues. The shear modulus for the soft biological tissues span a much larger range compared to the bulk modulus, by several orders of magnitude [23, 24]. Therefore, shear modulus measurement using the proposed shear wave OCT could potentially be used better differentiate tissue structures.

2. Acoustic Radiation Force

Acoustic radiation force is produced by a change in the energy density of the incident acoustic field [25, 26]. The acoustic radiation force is generated by the transfer of momentum from the acoustic wave to the tissue. The force is applied in the direction of the longitudinal wave propagation and the magnitude of the force can be approximated by:

$$F = \frac{2\alpha I}{C} \tag{1}$$

where F, kg/(s ^{2} cm ^{2}), is acoustic radiation force, c (m/s) is the speed of sound in the medium, α (Np/m) is the absorption coefficient of the medium and I (W/cm^2) is the temporal average intensity at a given spatial location[27]. Figure 1 shows the principle of shear wave generation. Shear waves can be generated by using a focused impulse generated by a transducer. The impulse creates a displacement in the direction of ultrasonic beam propagation which is largest at the focus of the transducer. Immediately after the impulse the material relaxes back to its original state producing a shear wave. The shear wave propagates in the direction perpendicular to the direction of the focused ultrasound propagation.

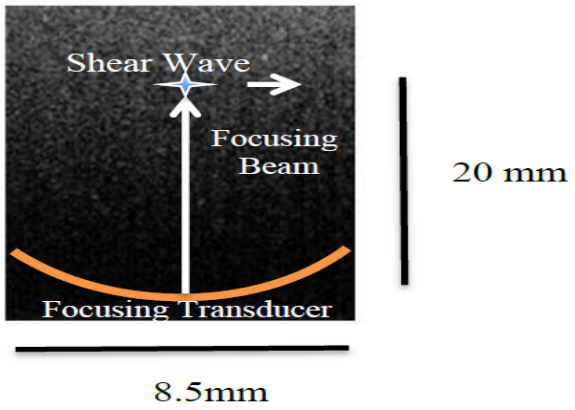

Figure 1.The principle of shear wave generation. Shear waves can be generated by using a focused impulse generated by a transducer.

2.1 Shear Moduli and wave propagation

By using the Voigt model for a homogenous medium, the shear wave speed C_s describes by following equation 2 which is related to the shear modulus μ_1, shear viscosity μ_2, shear wave angular frequency ω, and tissue density ρ as following [28,26, 29].

$$C_s(\omega)=\sqrt{2(\mu_1^2+\omega^2\mu_2^2)/\rho(\mu_1+\sqrt{\mu_1^2+\omega^2\mu_2^2})} \quad (2)$$

Experimentally, the displacements of shear waves at each tracking location are calculated based on a speckle tracking algorithm. The shear wave speed could be calculated using $\Delta\varphi$ and Δr calculated from the measured phase shift and the distance between the two tracking locations. Shear wave speed is calculated by the following equation.

$$C_s(\omega)=\frac{\omega\Delta r}{\Delta\varphi} \quad (3)$$

Where $\omega=2\pi f$, $\Delta\varphi$ *is* the phase shift and Δr *is* the distance between the two tracking locations.

To characterize the acoustic radiation force, the displacement of a rigid sphere intercepting an ultrasound beam can be analyzed. A rigid sphere scatters and absorbs a portion of the ultrasound wave incident upon it; the resulting medium displacement caused by the motion of the sphere [30-34] can be used to calculate the mechanical properties of the medium [35]. The motion of a sphere that is exposed to such a beam has been studied by Oestreicher [37], amongst other investigators [36-38]. It can be shown that the sphere motion caused by the acoustic radiation force is related to the viscoelastic properties of the medium, and that this motion can be analyzed to extract the local mechanical properties of the medium.

3. Materials and Methods

In this study, we present a dynamic excitation OCE technique using the ultrasound ARF. A custom swept-source OCT system was used in this study. The laser had a center wavelength of a 1310 nm and a bandwidth of ~110 nm. The lateral resolution was approximately 13 μm in the samples. Acoustic radiation force (internal mechanical excitation) was applied by a 20 MHz circular 8.5 mm diameter piezoelectric transducer element (PZT, f-number 2.35) transmitting sine-wave bursts of 400 μs. The PZT element push sequence was synchronized with the OCT imaging system.

In this study, we used two different samples. The first type of phantom consisted of a 355 μm glass sphere (dark) embedded in gelatin and was used to characterize the ultrasound pushing beam. The second phantom consisted of gelatin mixed with titanium dioxide which provided uniform acoustic and optical scattering. For both phantoms, Gelatin samples (Type B, Fisher Scientific, G7-500) were constructed to test the method. Gelatin powder and distilled water were heated in a water bath at 60−65 ^{0}C for one hour and periodically stirred. When the sample cooled to 40 ^{0}C, then for first phantom 0.1% weight by-weight (w/w) formaldehyde was added and thoroughly mixed. Liquid gelatin was poured into the sample mold (height 20 mm). A 355 μm glass sphere (dark) was introduced just prior to gelling. The sphere was used to characterize the ARF beam. For the second phantom, 0.1% weight by weight titanium dioxide (Sigma-Aldrich, Titanium(IV) oxide nanopowder, <25 nm particle size, 99.7% trace metals basis) was added and thoroughly mixed. Molten titanium dioxide – gelatin was poured into rectangle molds (20 mm height) and allowed to congeal. The titanium dioxide was used as a scattering agent.

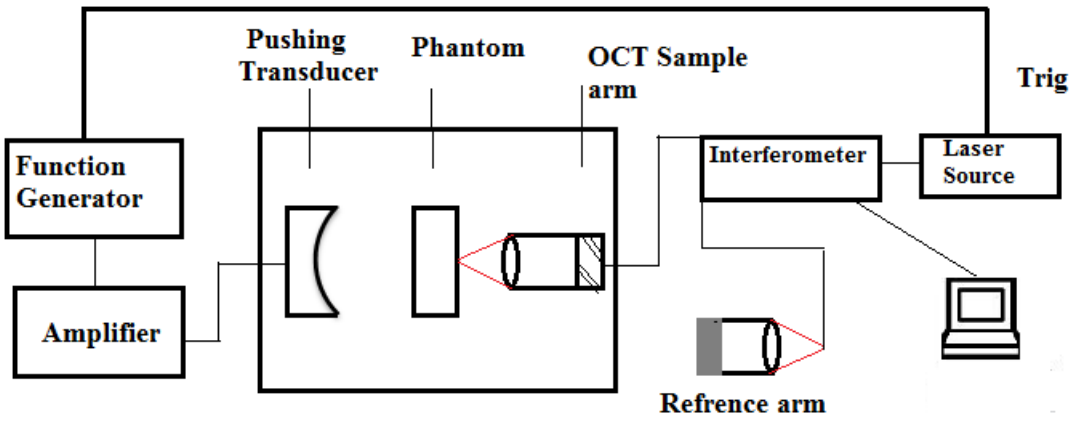

Figure 2. Schematic diagram of Acoustic Radiation Force-Optical Coherence Elastography (ARF-OCE). The experimental set-up consisted of a phantom, a focused transducer (20 MHz, f-number 2.35), a function generator (Agilent 33250A 80 MHz, Function / Arbitrary Waveform Generator) and an amplifier which was synchronized with the OCT system.

The OCT signal from this second set of phantoms was used for the measurement of the shear wave speed and viscosity. The ultrasound "push" transducer is synchronized with the OCT imaging system. For both sets of experiments phase analysis was applied to B-mode and M-mode OCT images which were obtained while ultrasound transducer was generating the "push" in the phantom. A fast Fourier transform was performed on the OCT data and phase maps of the phantom under ultrasound loading were generated, which are directly related to the acoustic radiation force induced displacement in the phantom**.**

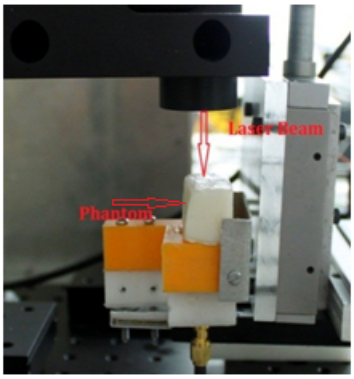

Figure 3.Experimental setup for imaging shear wave propagation. The OCT galvo scanner is at the top of the image, the 3D micrometer stage which is used for attaching the phantom to the pushing transducer is shown at the bottom.

4. Results and Conclusion

A B-mode OCT image of the sphere is shown in Figure 4a. The arrow in this figure denotes the position from where M-Mode OCT images were acquired. Figure 4b shows the phase of the M-mode OCE image, which is proportional to the displacement of the sphere over time.

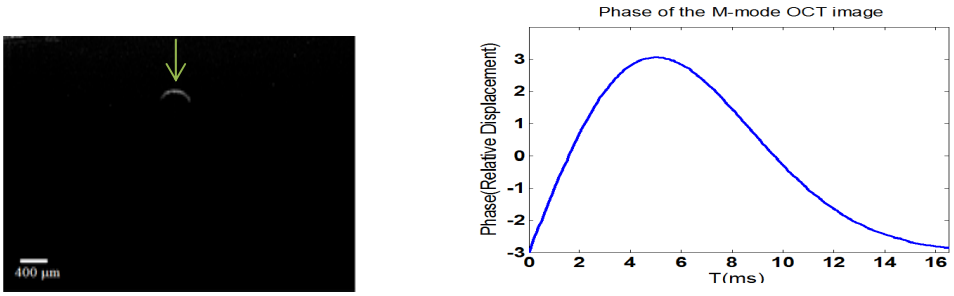

(a) **(b)**

Figure 4. (a):B-Mode structural OCT image of 355 µm glass sphere (dark) embedded in gelatin which was used to characterize the ultrasound pushing beam.(b): Phase measurement from surface of glass sphere during the ARF impulse and subsequent relaxation.

Figure 5 shows the B mode image of the titanium dioxide – gelatin phantom and the arrow denotes the position from which the M-mode OCT images were acquired.

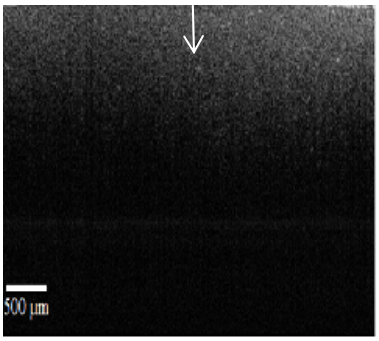

Figure 5.B-Mode structure image of the titanium dioxide – gelatin phantom (See Figure 6 for the corresponding phase map). The arrow denotes the position from which the M-mode OCT data were acquired.

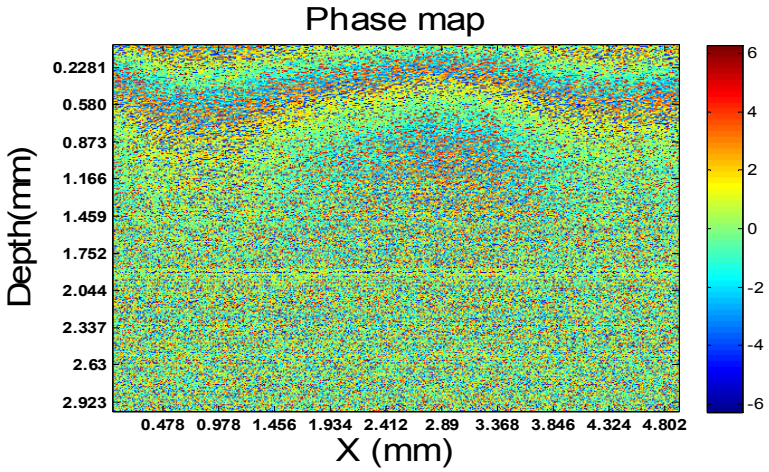

Figure 6.B-Mode phase map from the titanium dioxide – gelatin phantom used to measure Δr and $\Delta\varphi$ for the calculation of the shear wave speed. The color scale represents the change of the phase value.

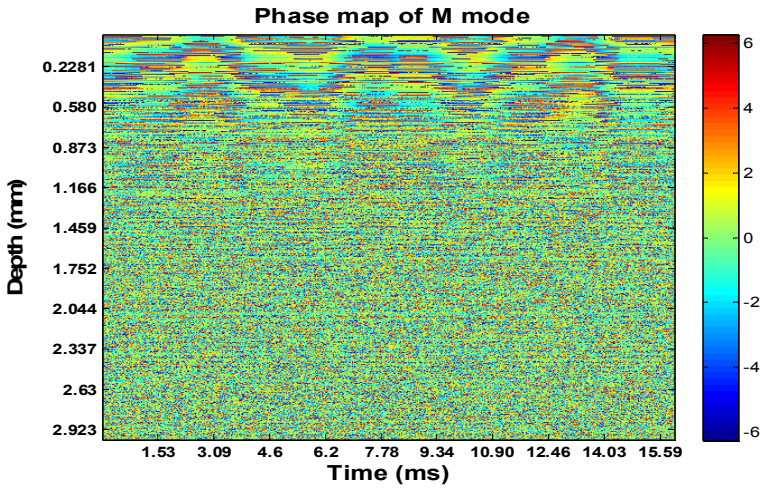

Figure 7.M-Mode phase map from the titanium dioxide – gelatin phantom used to calculate the shear wave frequency. The color scale represents the change of the phase value.

By calculating the time difference between successive peaks in the M mode dataset of Figure 7, the frequency of the shear wave was calculated to be approximately 266 Hz. The shear wave speed could then be calculated using Δr and $\Delta\varphi$ calculated from the measured phase shift and distance between the 2 successive peak locations which were obtained from Figure 6. These values were then used in equation 3 to calculate the shear wave speed. The shear wave speeds for the 14% and 8% gelatin - titanium dioxide phantoms were 2.24±0.059 m/s and 1.49± 0.046 m/s respectively (table A).

The Young's modulus and shear modulus were calculated from the experimental results using the following equation (which assumes an isotropic homogeneous medium):

$$C_s = \sqrt{\frac{\mu}{\rho}} \tag{4}$$

and

$$E = 3\mu = 3C_s^{\,2}\rho \tag{5}$$

where μ, E represents the shear modulus and Young's moduli respectively. The measured density ρ of the phantom samples was 1100 kg/m^3. Table A summarizes the Young's and shear moduli for both phantoms. The shear modulus estimated using OCE for phantom 1 was 5.51± 0.065 KPa and for phantom 2 was 2.44±0.051 KPa. The Young's modulus estimated using OCE for phantom 1 was 16.55± 0.195 KPa and for phantom 2 was 7.33± 0.153 KPa. As expected the values of the shear and Young's moduli were greater for the phantom with the higher concentration of gelatin.

Table (A): mechanical properties of phantoms.

Samples	Shear wave speed(C_s,m/s)	Shear modulus(μ, KPa)	Young modulus(E, KPa)
Sample1 (14%)	2.24±0.059	5.51± 0.065	16.55± 0.195
Sample 2 (8%)	1.49± 0.046	2.44±0.051	7.33± 0.153

In the summary, we have demonstrated a technique that uses acoustic radiation force for the mechanical excitation of a gelatin phantom. The mechanical excitation produces motion within the phantom that can use for the estimation of the phantom mechanical properties using OCE. This was achieved by measuring both the displacement of a sphere embedded in the gelatin phantom and the displacement in a homogeneous phantom using OCT phase maps. We conclude the

Optical Coherence Elastography can be used to measure the tissue stiffness properties by tracking tissue displacement after dynamic excitation. From the shear wave speed measurement, the Young's and shear moduli of the gelatin phantom mixed with titanium dioxide were calculated.

5. Acknowledgments

Marjan Razani is supported by an Ontario Graduate Scholarship (OGS). This work is funded in part by the Canada Research Chairs program (awarded to Drs. V.X.D. Yang and M. C. Kolios), the Natural Sciences and Engineering Research Council of Canada (NSERC discovery grant 216986-07) and Canada Foundation for Innovation. We would like to thank Dr. Mathias Fink and Arthur Worthington for their contributions and discussions.

6. References

[1] Ophir, J., Alam, S.K., Garra, B., Kallel, F., Konofagou, E., Krouskop, T. and Varghese, T., "Elastography: ultrasonic estimation and imaging of the elastic properties of tissues," Proc Inst Mech Eng H, 213(3), 203- 233 (1999).
[2] Sun, C., Standish, B. and Yang, V. X. D., "Optical coherence elastography: current status and future applications," Biomedical Optics, 16(4), 043001 (2011).
[3] Schmitt, J. M., "OCT elastography: imaging microscopic deformation and strain of tissue," Opt. Express, 3(6), 199-211 (1998).
[4] Liang, X., Orescanin, M., Toohey, K. S., Insana, M.F. Boppart1, S. A., "Acoustomotive optical coherence elastography for measuring material mechanical properties," Optics Letters, 34(19), 2894-2896 (2009).
[5] Greenleaf, J. F., Fatemi, M. and Insana, M., "Selected methods for imaging elastic properties of biological tissues," Annu. Rev. Biomed. Eng, 5 ,57-78 (2003).
[6] Fatemi, M. and Greenleaf, J. F., "Application of radiation force in noncontact measurements of the elastic parameters," Ultrason. Imaging, 21(2), 147-154 (1999).
[7] Hachemi, M. E., Calle, S. and Remenieras, J. P.,"Transient displacement induced in shear wave elastography: Comparison between analytical results and ultrasound measurements," Ultrasonics, 44(22), 221-225 (2006).
[8] Ostrovsky, L., Sutin, A., Il'inskii, Y., Rudenko, O. and Sarvazyan, A., "Radiation force and shear motions in inhomogeneous media,"J. Acoust. Soc. Am, 121(3), 1324-1331 (2007).
[9] Palmeri, M. L., McAleavey, S. A., Fong, K. L., Trahey, G. E. and Nightingale, K. R., "Dynamic mechanical response of elastic spherical inclusions to impulsive acoustic radiation force excitation," Ultrasonics. Ferroelectrics and Frequency Control. IEEE Transactions on, 53(11), 2065-2079 (2006).
[10] Walker, W. F., Fernandez, F. J. and Negron, L. A., "A method of imaging viscoelastic parameters with acoustic radiation force," Phys.Med. Biol, 45(6), 1437-1447 (2000).
[11] Nightingale, K., Soo, M. S., Nightingale, R. and Trahey, G., "Acoustic radiation force impulse imaging: In vivo demonstration of clinical feasibility," Ultrasound Med Biol, 28(2), 227-235 (2002).
[12] Nightingale, K. R., Nightingale, R. W., Stutz, D. L. and Trahey, G. E., "Acoustic radiation force impulse imaging of in vivo Vastus Medialis muscle under varying isometric load," Ultrasonic Imaging, 24,100-108 (2002).
[13] Fatemi, M. and Greenleaf, J. F., "Ultrasound-stimulated vibro-acoustic spectrography," Science, 280(5360), 82-85 (1998).
[14] Nightingale, K., Palmeri, M. and Trahey, G., "Analysis of contrast in images generated with transient acoustic radiation force," Ultrasound Med. Biol, 32(1), 61-72 (2006).
[15] Bercoff, J., Tanter, M. and Fink, M., "Supersonic shear imaging: A new technique for soft tissue elasticity mapping," Ultrasonics, Ferroelectrics and Frequency Control, IEEE Transactions on, 51(4), 396 - 409 (2004).
[16] Nightingale, K., McAleavey, S. and Trahey, G., "Shear wave generation using acoustic radiation force: In vivo and ex vivo results,"Ultrasound Med. Biol, 29(2), 1715-1723 (2003).
[17] Palmeri, M. L., McAleavey, S. A., Trahey, G. E. and Nightingale, K. R., "Ultrasonic tracking of acoustic radiation force-induced displacements in homogeneous media,"Ultrasonics. Ferroelectrics and Frequency Control. IEEE Transactions on, 53(7), 1300–1313 (2006).
[18] Pinton, G. F. and Trahey, G. E., "Continuous delay estimation with polynomial splines," Ultrasonics. Ferroelectrics and Frequency Control. IEEE Transactions on, 53(11), 2026-2035 (2006).
[19] McLaughlin, J. and Renzi, D., "Shear wave speed recovery in transient elastography and supersonic imaging using propagating fronts,"Inverse Probl, 22, 681-706 (2006).

[20] McLaughlin, J. and Renzi, D., "Using level set based inversion of arrival times to recover shear wave speed in transient elastography and supersonic imaging," Inverse Probl, 22, 707-725 (2006).
[21] Palmeri, M . L., Wang, M. H., Dahl, J. J., Frinkley, K. D. and Nightingale, K.R., "Quantifying hepatic shear modulus in vivo using acoustic radiation force," Ultrasound Med. Biol, 34(4), 546-558 (2008).
[22] Karpiouk, A., Aglyamov, S., Ilinskii, Y., Zabolotskaya, E., Emelianov, S., "Assessment of Shear Modulus of Tissue Using Ultrasound Radiation Force Acting on a Spherical Acoustic Inhomogeneity," Ultrasonics. Ferroelectrics and Frequency Control. IEEE Transactions on, 56(11) (2009).
[23] Sarvazyan, A. P., Rudenko, O. V., Swanson, S. D., Fowlkes, J. B. and Emelianov, S. Y., "Shear wave elasticity imaging: A new ultrasonic technology of medical diagnostics," Ultrasound in Medicine & Biology, 24(9), 1419-1435 (1998).
[24] Orescanin, M., "Complex shear modulus reconstruction using ultrasound" Thesis, 1-185 (2010)
[25] Fatemi, M. and Greenleaf, J. F., "Vibro-acoustography: An imaging modality based on ultrasound-stimulated acoustic emission," Proc. Natl. Acad. Sci. USA, 96(12), 6603-6608 (1999).
[26] Chen, S., Fatemi, M. and Greenleaf, J. F., "Quantifying elasticity and viscosity from measurement of shear wave speed dispersion," J. Acoust. Soc. Am, 115(6), 2781-5 (2004).
[27] Nightingale, K. R., Bentley, R., Trahey, G.E., "Observations of tissue response to acoustic radiation force: opportunities for imaging", Ultrasonic Imaging, 24, 100-108 (2002).
[28] Yamakoshi,Y., Sato, J., Sato,T., "Ultrasonic imaging of internal vibration of soft tissue under forced vibration,". Ultrasonics. Ferroelectrics and Frequency Control. IEEE Transactions on, 37(2), 45-53 (1990).
[29] Chen, S., Fatemi, M. and Greenleaf, J. F., "Remote measurements of material properties from radiation force including vibrations of an embedded sphere," J. Acoust. Soc. Am, 112 (3 Pt1), 884-889 (2002).
[30] Skovoroda, A. R. and Sarvazyan, A. P., "Determination of viscoelastic shear characteristics of a medium from its response to focused ultrasonic loading," Biophysics (Oxf.), 44, 325-329 (1999).
[31] Sarvazyan, A. P., Rudenko, O. V., Nyborg, W.L., "Biomedical applications of radiation force of ultrasound: Historical roots and physical basis," Review. Ultrasound in Medicine and Biology, 36(9), 1379-1394 (2010).
[32] Bercoff, J., Tanter, M., Muller, M. and Fink, M., "The role of viscosity in the impulse diffraction field of elastic waves induced by the acoustic radiation force," IEEE Trans. Ultrason. Ferroelectr. Freq.Control, 51(11), 1523-1536 (2004).
[33] Calle, S., Remenieras, J. P., Matar, O. B., Hachemi, M. E. and Palat, F., "Temporal analysis of tissue displacement induced by a transient ultrasound radiation force," J. Acoust. Soc. Am, 118(5), 2829–2840 (2005).
[34] Walker, W. F., "Internal deformation of a uniform elastic solid by acoustic radiation force," J. Acoust. Soc. Am, 105(4), 2508–2518 (1999).
[35] Erpelding, T. N., Hollman, K. W. and O'Donnell, M., "Mapping age-related elasticity changes in porcine lenses using bubble-based acoustic radiation force," Exp Eye Res, 84(2), 332–341(2007).
[36] Aglyamov, S. R., Karpiouk, A. B., Ilinskii, Y. A., Zabolotskaya, E. A. and Emelianov, S. Y., "Motion of a solid sphere in a viscoelastic medium in response to applied acoustic radiation force: Theoretical analysis and experimental verification," J. Acoust. Soc. Am,122(4), 1927–1936(2007).
[37] Oestreicher, H. L., "Field and impedance of an oscillating sphere in viscoelastic medium with an application in biophysics," J. Acoust .Soc. Am, 23(6), 707–714, (1951).
[38] Ilinskii, Y. A., Meegan, G. D., Zabolotskaya, E. A. and Emelianov, S. Y., "Gas bubble and solid sphere motion in elastic media in response to acoustic radiation force," J. Acoust. Soc. Am,117(4), 2338–2346(2005).